Volume 1 | Number 1 | Jan 2013 | Pages 1–100

Journal of
Materials Chemistry B

Materials for biology and medicine
www.rsc.org/materialsB

ROYAL SOCIETY OF CHEMISTRY

ROYAL SOCIETY OF CHEMISTRY

www.rsc.org/materialsB

Journal Name

ARTICLE

Highly stable intrinsically radiolabeled indium-111 quantum dots with multidentate zwitterionic surface coating: dual modality tool for biological imaging

Minghao Sun, Gobalakrishnan Sundaresan, Purnima Jose, Likun Yang, David Hoffman, Narottam Lamichhane and Jamal Zweit*

Here we describe a novel strategy to incorporate indium-111 into near infrared (NIR) emitting Cu-In-Se quantum dots (CIS-QDs) to synthesize intrinsically radiolabeled QDs (rQDs), as a quantitative tool for *in vivo* SPECT/Fluorescence imaging. Multidentate zwitterionic polymer ligands were used to functionalize and improve the stability of CIS-rQDs and reduce nonspecific binding with plasma proteins/cell membrane. CIS-rQDs were taken up by colorectal adenocarcinoma (COLO-205) and human epidermoid carcinoma (KB-3-1) cells at low uptake rate (~0.4%, 2×10^5 QDs/cell at 24 hrs) and reduced nonspecific interaction of zwitterionic CIS-rQDs with cells was observed by fluorescence microscopy. The cytotoxicity of CIS-rQDs was reduced due to the low toxic inorganic composition of QDs and multidentate zwitterionic surface coating. In 5 out of 6 nude mice bearing either COLO-205 or KB-3-1 tumor, both SPECT and fluorescence imaging demonstrated passive localization of CIS-rQDs in the tumor as early as 6 hrs post-injection. In these mice the passive accumulation of CIS-rQDs in the tumor, due to leaky vasculature, ranged from ~0.3% ID/g to ~4.6% ID/g at 48 hrs post-injection (from region of interest analysis of SPECT imaging). This intrinsic radio-labeling strategy provides a nanoparticle platform which incorporates imaging and potentially therapeutic radionuclides with retention of fluorescence intensity. It also provides complimentary quantitative data capabilities for both *in vivo* SPECT imaging and radiotracer *ex vivo* analysis.

Introduction

Multimodal molecular imaging is becoming an active field due to its extensive biomedical applications in noninvasive disease diagnosis.[1] A number of hybrid nanoparticles (NPs) have been developed as contrast agents for multimodal molecular imaging. For example, iron oxide NPs combined with organic dyes/radiolabeled chelator/quantum dots (QDs) have been used as magnetic resonance (MR)/fluorescence/positron emission tomography (PET) imaging probes.[2-5] Gold NPs combined with paramagnetic iron oxide NPs or gadolinium chelators have been used for X-ray computed tomography (CT)/MR or photoacoustic/MR/Raman imaging.[6,7] Quantum dots, due to their unique optical properties, have been considered as the most promising fluorescent nanoprobes for optical imaging.[8-10] Hybrid QDs functionalized with gadolinium or radionuclides through chelation chemistry have been used as MR/fluorescence or fluorescence/PET imaging nanoprobes previously.[11-15] However, cadmium-based QDs, suffer from inherent cadmium toxicity, which limits their biological applications. NIR emission cadmium-free QDs attracted more attention due to their lower toxicity and less background interference in imaging window for biomedical applications.[16-21]

A unique advantage of inorganic, and inherently signaling NPs, is that many of them are made of (or can be doped with) elements that are compatible with bioinorganic radionuclides (SPECT/PET imaging and therapy radioisotopes), paramagnetic metals (MR imaging), or exogenous X-ray or optoacoustic (OA) responsive components (such as noble metal NPs for X-ray or ultrasonic/photoacoustic imaging). Combination of fluorescence with SPECT/PET, MR, or OA signals capitalizes not only on the strengths of the individual modality, but more importantly provides a platform for multiple pathways targeting and imaging of disease and its microenvironment. Overcoming optical depth and quantitative capability limitations, by incorporating radionuclides and/or contrast agents, will help cross validate and provide more comprehensive interpretation of combined image data. At the preclinical level, the advantage of optical imaging, such as multiplexing and high sensitivity, low cost, simplicity and accessibility can be robustly validated by quantitative tomographic imaging of SPECT/CT, PET/CT or PET/MR. Such a strategy will accelerate clinical translational research with more clinically applicable imaging modalities, like radionuclide-based and MR imaging. Chelator radiolabeling strategy has been developed to synthesize extrinsically radioactive QDs (rQDs). However, extrinsically rQDs did not show high stability *in vivo* and pharmacokinetics

of NPs could be potentially influenced by radiolabeling strategy itself.[14,22] Recently, we have developed a strategy to intrinsically incorporate radionuclides into NPs to yield "intrinsic" radiolabeled nanoprobes with high bio-stability.[23,24]

Surface modifications play a crucial role in the overall pharmacokinetics of NPs. We have demonstrated that different surface modification resulted in different pharmacokinetics of radiolabeled NPs. For example, compared with PEGylated rQDs, zwitterionic functionalized rQDs showed obvious prolonged blood circulation and reduced RES accumulation.[23] Monodentate molecular ligands coated QDs suffer from poor stability *in vivo* due to their interaction with enzymes and proteins in blood plasma, as well as intracellular thiol-compounds such as glutathione.[25] Multidentate macromolecules or biomacromolecules based ligands have been used as a more efficient platform to achieve highly stable, multifunctional water-soluble NPs.[26-28] Although multidentate Poly-PEG ligands have been used to functionalize QDs and other NPs,[29,30] reports on the synthesis and effect of surface modification of NPs with multidentate zwittererionic ligands are limited.[31]

In this paper, we synthesized a highly stable, intrinsically radioactive, near infrared emission indium-based QDs by doping ^{111}In in crystal structure of NPs (CIS-rQDs). Multidentate zwitterionic polymer ligands were used to functionalize CIS-rQDs through reaction in micro-emulsion solution to achieve a highly stable biocompatible CIS-rQDs. Zwitterionic surface functionalization of CIS-rQDs reduced the nonspecific interaction of NPs with plasma proteins and cell membrane. SPECT/fluorescence images indicated high stability of the bimodal nanoprobes *in vivo*. Radiotracer accumulation of the CIS-rQDs in tumor through the enhanced permeation and retention (EPR) effect was demonstrated in individual tumor by SPECT/ fluorescence imaging. This novel bimodal CIS-rQDs provides a promising non-invasive platform to study NP tissue-based pharmacokinetic and toxicity profiles *in vivo*.

Experimental section

Chemicals

All chemicals were used as received without further purification. Copper (I) chloride (99.99%), indium (III) chloride (99.999%), selenourea (98%), trioctylphosphine (TOP, 90%), 1-octadecene (ODE, 90%), oleylamine (OA, tech grade), dioctylamine (DOA, 98%), 1-dodecanethiol (DDT, 98%), zinc oxide (99%), poly(acrylic acid) (PAA, Mw = 1,800), lipoic acid (LA) (95%), carbonyldiimidazole (CDI, reagent grade), ethylenediamine (98%), 1,3-propane sultone (95%), sodium 1,1',3,3,3',3'-hexamethylindotricarbocyanine iodide (HITCI, 97%), sodium borohydride (96%), and poly(styrene-co-allyl alcohol) (Ps-co-Paa, Mw = 2,200) were purchased from Sigma-Aldrich. N,N'-dimethylethylenediamine (DMEDA, 95%) was obtained from Alfa Aesar. Zinc ethyl xanthogenate and zinc oleate were prepared according to published methods.[27] [111]InCl₃ solution in 0.05M HCl (specific activity: 458mCi/mg) was purchased from Perkin Elmer.

Characterization

Transmission electron microscopy (TEM) images were recorded on JEOL JEM-1230 transmission electron microscope operating at an accelerating voltage of 120 KV. The samples were prepared by dropping diluted solution of CIS-rQDs in toluene on the carbon film supported copper grids (Formvar/Carbon 300 Mesh Cu). Zeta Sizer Nano Series

ZEN3600 was used to measure the hydrodynamic (HD) size and zeta potential of CIS-rQDs in water or PBS buffer. UV-vis absorption and fluorescent emission spectra of CIS-rQDs in solution were recorded by Hewlett Packard 8453 and Varian Cary eclipse spectrophotometer respectively. The radioactive reaction yield was calculated from gamma counting. ^{1}H and ^{13}C NMR spectra were recorded on Varian Mercury 300 spectrometer with solvent proton resonance as reference. Inductively coupled plasma (ICP) measurement was carried on Vista-MPX CCD Simultaneous ICP-OES (Varian) with nitric acid solution of samples and CIS-rQDs was digested in nitric acid (7%) for three days before measurement.

Synthesis of CIS-rQDs

Copper (I) chloride (10 mg, 0.1 mmol), indium (III) chloride (22 mg, 0.1 mmol), and selenourea (25 mg, 0.2 mmol) were added into a 25 mL three-neck flask with 1-octadecene (2.5 mL) and trioctylphosphine (1.0 mL). The mixture was sonicated 30 min then oleylamine (1.0 mL) and 1-dodecanethiol (0.5 mL) were added. Mixture was stirred and degassed 30 min under vacuum then purged with argon. Reaction solution was heated to 50-60 °C overnight under the argon and stirring. The clear colorless solution was cooled down to r.t. then heated to 200°C. The color of reaction solution changed from yellow to red then black which indicated the nucleation and growth of nanocrystal. Heating was stopped immediately after the temperature reached to 200 °C and the reaction mixture was allowed to cool down to r.t. CIS-QDs was precipitated by the mixture of acetone (5 mL) and methanol (10 mL) and collected after centrifugation (6,000 rpm). The pellet was dissolved in 10 mL chloroform.

[111]InCl₃ (7 mCi, specific activity: 415.8 mCi/mg) aqueous solution was loaded in a 25 mL three-neck flask. Water was carefully removed under heating and argon flow. The solution of CIS-QDs in chloroform (5 mL), 1-octadecene (2 mL) and oleylamine (0.5 mL) was loaded into the flask. Chloroform was removed under vacuum at 60 °C. Solution (0.5 mL) of zinc bis(ethyl xanthogenate) (30 mg) and zinc oleate (250 mg) in the mixture of ODE (1.0 mL), TOP (1.5 mL) and DOA (0.5 mL) was added into the reaction mixture and the temperature was increased to 190 °C. Rest Zn precursor solution was added dropwise into the reaction mixture within 1 hr at 190 °C. The reaction mixture then was cooled down to r.t. Acetone/methanol (1/3) was used to precipitate CIS-rQDs. The cloudy solution was centrifuged at 6,000 rpm for 5 min and the pellet was collected. Chloroform (10 mL) was added to dissolve the pellet and the solution was filtrated through 0.2 μm nylon filter. Radioactive reaction yield: 92%. Specific activity of CIS-rQDs: ~125 Ci/mmole.

Synthesis of zwitterionic ligands and ligand exchange

Synthesis of bidentate zwitterionic ligands DHLA-SB and multidentate zwitterionic ligands PAA-DHLA-SB and ligand exchange were followed according to previous procedure.[23, 42] Molecular structure of DHLA-SB and synthetic route of PAA-DHLA-SB were shown in Fig. 1b.

Synthesis of DHLA-SB. To a lipoic acid solution (2 g, 9.7 mmole) in chloroform (10 mL) was added CDI (1.88 g, 11.6 mmole) and stirred for 30 min under argon. The final solution was added dropwise to the solution of N, N-dimethylethylenediamine (1.28 mL, 11.6 mmole) in chloroform (20 mL) at 4 °C under argon. The reaction mixture was stirred overnight at r.t. The product was washed with brine (15 mL×3) followed by aqueous NaOH solution (15 mL×3, 10 mM). The

ARTICLE

organic phase was dried over anhydrous Na_2SO_4. Removal of organic solvent yields **LA-DMN** as a yellow oil (2.4 g, 90%). ^{1}H NMR (300 MHz, $CDCl_3$, 25 °C, TMS): 5.98 (s, 1H), 3.57 (m, 1H), 3.34-3.28 (t, 2H), 3.21-3.06 (m, 2H), 2.50-2.37 (m, 3H), 2.22 (s, 6H), 2.18 (t, 2H), 1.96-1.85 (m, 1H), 1.74-1.62 (m, 4H), 1.52-1.43 (m, 2H) ppm. ^{13}C NMR (75 MHz): 58.06, 56.63, 45.30, 40.42, 38.65, 36.84, 36.55, 34.82, 29.09, 25.60 ppm.

To a solution of **LA-DMN** (0.51 g, 1.85 mmole) in chloroform (10 mL) was added 1,3-propane sultone (0.236 g, 1.93 mmole). The reaction was kept at 60 °C under argon and stirred overnight. The yellow precipitate was filtered and washed by chloroform (15 mL×3). The product was dried under vacuum to give **LA-SB** as a yellow solid (0.56g, 76%). ^{1}H NMR (300 MHz, D_2O, 25 °C): 3.70 (t, 2H), 3.62-3.49 (m, 5H), 3.23 (m, 2H), 3.19 (s, 6H), 3.00 (t, 2H), 2.50 (m, 1H), 2.34-2.24 (m, 4H), 2.03 (m, 1H), 1.79-1.60 (m, 4H), 1.49-1.41 (t, 2H), 1.20 (t, 1H) ppm. ^{13}C NMR (75 MHz): 177.08, 63.00, 61.85, 56.74, 51.15, 49.00, 47.38, 40.53, 38.45, 35.53, 34.06, 33.21, 28.29, 25.04, 18.40 ppm.

To a solution of **LA-SB** (0.56 g, 1.44 mmole) in a mixture of water (12 mL) and ethanol (3 mL) was added $NaBH_4$ (62 mg, 1.68 mmole) aliquot at 4 °C. The reaction was gradually warmed to r.t and kept for 4 hrs. After removal of the solvent, the product was obtained as a white solid without further purification. 20 mL water was added to dissolve **DHLA-SB** and the solution was used for ligand exchange reaction directly. ^{1}H NMR (300 MHz, D_2O, 25 °C): 3.72 (t, 2H), 3.59-3.50 (m, 4H), 3.20 (s, 6H), 3.02 (m, 3H), 2.67 (m, 2H), 2.40-2.25 (m, 5H), 1.90-1.47 (m, 10H) ppm.

Synthesis of PAA-DHLA-SB. The solution of PAA (0.5 g, 0.27 mmole) in anhydrous THF (10 mL) was transferred to the solution of CDI (1.24 g, 7.65 mmole) in anhydrous THF (10 mL) under Ar at r.t. The reaction was kept 12 hrs at r.t. under stirring to form clear solution. The above activated PAA solution was dropwised into the mixture of amino-lipoic acid (1) (1.14 g, 4.6 mmole) and DMEDA (2) (0.2 g, 2.3 mmole,) under Ar at 4 °C. The reaction solution was kept overnight at r.t. under stirring. The product was washed by brine three times. Combined organic phase was dried by anhydrous Na_2SO_4. Removal of organic solvent gives the crude product as yellow solid. The crude product was purified by size exclusive chromatography with THF as mobile phase to give polymer **PAA-LA-DMN** (0.67 g, 45%). ^{1}H NMR (300 MHz, $CDCl_3$, ppm): δ 4.3 (broad), 4.1-3.7 (broad), 3.5 (broad), 3.3 (broad), 3.1 (broad), 2.5-2.4 (broad), 2.2 (broad), 2.0-1.8 (broad), 1.6-1.3 (broad), 1.3-1.2 (broad).

To a solution of **PAA-LA-DMN** (0.67 g) in chloroform (10 mL) was added 1,3-propane sultone (0.13 g, 1.1 mmole). Reaction was kept at 65 °C under Ar and stirred overnight. The yellow precipitate was collected through filtration and washed by chloroform three times (3×15 mL). The product was dried under the vacuum to give **PAA-LA-SB** as slightly yellow solid (0.67 g, 86%). ^{1}H NMR (300 MHz, D_2O, ppm): δ 4.6 (broad), 4.2 (broad), 3.7 (broad), 3.6 (broad), 3.5 (broad,), 3.2 (broad), 3.0 (broad), 2.7 (broad), 2.5 (broad), 2.3 (broad), 2.0 (broad), 1.7-1.3 (broad).

To a solution of **PAA-LA-SB** in H_2O/ethanol (15 mL, v/v = 4/1) was added sodium borohydride aliquot at 4 °C. Reaction was kept at r.t. under stirring for 4 hrs. The solvent was removed under vacuum. 20 mL water was added to dissolve residue and solution was filtrated. No further purification was performed to the product. The solution of **PAA-DHLA-SB** in H_2O was directly used for ligand exchange reaction. ^{1}H NMR (300 MHz, D_2O, ppm): δ 4.6 (broad), 3.7 (broad), 3.6 (broad),

3.2 (broad), 3.0 (broad), 2.7 (broad), 2.5 (broad), 2.3 (broad), 2.0 (broad), 1.7-1.2 (broad).

Ligand exchange. Three-component micro-emulsion method was used for ligand exchange reaction of CIS-rQDs with PAA-DHLA-SB. The reaction was performed in two-phase system. Amphiphilic copolymer Ps-*co*-Paa was added to the solution of rQDs (6 nmole) in chloroform (3 mL) under Ar. Aqueous solution of polymer ligands (50 mg) in water (1 mL) was added into the above mixture under rigorously stirring. Two-phase reaction mixture was stirred under 45 °C. The two-phase solution was divided into two layers after quiescence and cooling to r.t. Water (1 mL) was added and the QDs aqueous solution was filtrated through 0.2 μm nylon filter. The filtrated solution was centrifuged to separate over excess ligands and concentrated over Amicon filters (30,000 MWCO) at 10,000 rpm for 30 min.

Inductively Coupled Plasma (ICP) measurement

CIS-rQDs was diluted by 7% nitric acid solution (trace metal content nitric acid in nanopure water) and digested for 3 days to completely dissolve CIS-rQDs. The concentration of indium, copper and selenium (ppm) was calculated based on the calibrated standard curve respectively. Atomic absorption peaks of indium at 325.609 nm, copper at 327.395 nm and selenium at 196.026 nm were selected to measure the concentration of different elements.

Stability study of CIS-rQDs in mouse serum by gel filtration chromatography (GFC)

Zwitterionic CIS-rQDs was analyzed by HPLC on an 8 x 300 mm, TSK gel-G3000SW (TOSOH Bioscience, Japan) gel filtration column. Mobile phase containing 0.05M Na_2HPO_4, 0.05M NaH_2PO_4 and 0.15M NaCl was used as the eluent. Flow rate of mobile phase is 1.0 mL/min. CIS-rQDs in saline (25 μL, 5 μCi) was injected into Radio-HPLC-GFC. Calibration of HD size of CIS-rQDs was performed by injecting 10 μL of gel filtration protein standards from Bio-Rad containing thyroglobulin (669 kDa, 18.8 nm HD), γ-globulin (158 kDa, 11.1 nm HD), ovalbumin (44 kDa, 6.1 nm HD), myoglobin (17 kDa, 3.8 nm HD), and vitamin B12 (1.4 kDa, 1.67 nm HD). On-line, full spectrum analysis of UV-vis absorbance (model 2489, Waters) and radioactivity (model B-FC-3300, bio-scan) permits monitoring the retention time of zwitterionic CIS-rQDs simultaneously.

CIS-rQDs (40 μL, 1 μCi/ μL) saline solution was incubated with mouse plasma (1 mL) at 25°C at different time points (2 hrs, 4 hrs, 6 hrs and 24 hrs), 200 μL incubated solution (CIS-rQDs in plasma) was injected into HPLC and the retention time of samples was monitored by Bioscan Model 106 radiation detector and compared with neat CIS-rQDs.

Quantum yield measurement of zwitterionic CIS-rQDs

Quantum yield (QY) of zwitterionic CIS-rQDs in water was measured relative to HITCI (in methanol) under excitation of 650 nm. Solutions of CIS-rQD in water and dye in methanol were optically matched at the excitation wavelength. The UV-vis absorption density was kept below 0.1 between 450-900 nm. The integration of emission spectra, corrected for differences in index of refraction and concentration, were used to calculate the QY using following expression: $QY_{QD} = QY_{Dye} * (Absorbance_{dye}/Absorbance_{QD}) * (Peak\ Area_{QD}/Peak\ Area_{dye}) * (n_{QD-solvent})^2/(n_{dye-solvent})^2$.

In vitro cellular response

Human cervical carcinoma (KB-3-1) and colorectrectal adenocarcinoma (COLO-205) cell lines were maintained in humidified incubator at 37°C and 5% CO_2. KB-3-1 cells were grown in DMEM/High glucose medium supplemented with 10% fetal bovine serum (FBS), 5mM L-Glutamine, Penicillin (100U/ml), Streptomycin (100µg/ml) and Amphotericin B (0.25 ug/ml). COLO-205 cells were cultured in RPMI-1640 medium supplemented with 10% heat inactivated FBS Penicillin G (100 U/ml), Streptomycin (100 µg/ml) and Amphotericin B (0.25 µg/ml). The cells were grown to 70-80% confluency before using for the experiments.

The cell viability of KB-3-1 and COLO-205 cells treated with zwitterionic CIS-rQDs was evaluated using a Cell TiterGlo assay kit (Promega, USA). Briefly, 10^4 cells were plated in opaque 384-well plate in triplicates for each cell type and treated with various concentrations of zwitterionic CIS-rQDs for 24 hrs. At the end of incubation period the assay reagent was added, and the cell viability was assessed by measuring the luminescence, detected by a plate reader (Beckman Coulter). The luminescence detected in untreated cells was used as control (100% Viability) to calculate percent viability in each treatment groups. Statistical analysis was done using Student's t-test and the p value calculated based on two-tailed test using Microsoft Excel software. $P<0.05$ was considered statistically significant.

To study the accumulation of zwitterionic CIS-rQDs with time in COLO-205 and KB-3-1 cells, 600-800K cells were seeded in 6-well plate in 10% complete growth medium and allowed to adhere overnight. After overnight culture, the used culture medium was replaced with 1% serum containing complete growth medium. The cells were then treated with 15 nM zwitterionic CIS-rQD for indicated periods of time. At the end of incubation period the supernatant was collected and an aliquot of it was used for gamma counting. The cells in the plate were thoroughly and gently rinsed with PBS and the wash buffer was collected and spun down to collect any non-adherent/loosely adherent cells in the wash and finally mixed with the adherent cells. The adherent cells in the plate were lysed using RIPA buffer (Pierce). An aliquot of the cell lysate was used for gamma counting and for measuring the amount of protein in each well. The amount of protein in each cell lysate was measured using BCA Protein assay kit (Pierce). The amount of uptake of CIS-rQDs/cell for each treatment group was calculated and statistical analysis was done using ANOVA and Fisher's PLSD post-hoc test done at 5% significance level using STAT view software.

Tumor Models

Human cervical carcinoma or colorectrectal adenocarcinoma was xenograft to female nude mice. Tumor xenografts were obtained by s.c. injection of $5×10^6$ cells with matrigel (50 µL) into the right flank of female nude mice. Mice bearing tumors (12.2 mm× 18.5 mm) weighing about 20-30 g were used for SPECT studies.

Fluorescent microscopy of cells

The interaction of CIS-rQDs with cells was studied by fluorescent microscopy. KB 3-1 and COLO 205 cells (0.2 x 10^6 cells) were seeded in chamber slides (thermo fisher) in 10% complete growth medium and allowed to adhere overnight. After overnight culture, the medium was replaced with 1%

serum containing complete growth medium. Then the cells were incubated with CIS-rQDs at 15 nM or 75 nM for 2 hrs or 24 hrs. The cells were then washed three times with PBS gently and fixed with 4% paraformaldehyde. Zwitterionic CIS-rQDs labeled cells were imaged under inverted fluorescence microscope, Olympus IX-71 with built-in Nuance Multispectra Image System (Perkin Elmer, USA) with excitation of TRITC channel (excitation: 530 nm/565 nm, emission: 580 nm to 720 nm).

In vivo/ex vivo fluorescence imaging

Animal experiments were approved and performed according to the policies and guidelines of the Animal Care and Use Committee (IACUC) at Virginia Commonwealth University. Nude mice were injected intravenously via the tail vein with zwitterionic CIS-rQDs at a dosage of 2.4 nmole. At different time points (6 hrs, 24 hrs and 48 hrs) post-injection of CIS-rQDs, NIR fluorescent multispectral images of mice were obtained using the Maestro-2 in vivo Imaging System (Perkin-Elmer, MA). A combination of excitation (684 to 729 nm band-pass) and emission (745 nm long-pass) filters with the acquisition settings of 740-950 in 10 nm increments was used to capture the NIR emission from CIS-rQDs. The resultant multispectral images were unmixed into their component spectra (CIS-rQDs, auto fluorescence, and background) using the in-built software. Following in vivo imaging at 48 hrs, mice were sacrificed and dissected tumor samples were imaged ex vivo with the same acquisition and unmixing settings.

In vivo SPECT/CT imaging

Micro-SPECT was performed using a multimodal (DPET/SPECT/CT) preclinical imaging system (Siemens, USA) having dual-head camera mounted with 2 multipinhole collimators (five 1.0-mm pinholes in each collimator, 51-mm trasaxial FOV, 40-mm radius of rotation and maximum resolution of 1.5 mm). Images were acquired over 360° in a total of 40 projections, resulting in a total imaging time of 30 min. Nude mice were intravenously injected with CIS-rQDs (300 µCi, 600 µL, 2.4 nmole) and 6 hrs later, were anesthetized with mixture of 2% isoflurane in oxygen and whole body micro-SPECT imaging was carried out in prone position as described above. Micro-CT was also performed with 75 kV and 500 µA at a resolution of 96 µm. The whole body scan time was 6 min. SPECT/CT images were acquired at 6, 24 and 48 hrs post injection of CIS-rQDs. The SPECT images were reconstructed using an iterative reconstruction algorithm (ordered-subset expectation maximization or OSEM3D) modified for the 5-pinhole geometry with a 20% energy window around the 171 keV photo peak of [111]In. These images were then registered with CT images based on a transformation matrix previously generated using four 57Co landmarkers. Images were viewed and quantified using the image data analysis software (ASIpro). Corrections for scatter and attenuation were not applied to the SPECT images.

In vivo magnetic resonance imaging

Mice were evaluated under magnetic resonance imaging (MRI) for comparing the degree of interstitial fluid accumulation inside tumors. MRI was performed with Bruker-Biospin Biospec console and a 7 Tesla, 30 cm free bore magnet. Animals were anesthetized with isoflurane during preparation

(2%) and imaging (1%). They were placed in a 35 mm I.D. birdcage coil tuned to 300 MHz. T2 weighted spin echo images were acquired in the axial plane with a field of view of 3.0 x 3.0 cms in a 130 x 130 matrix. Slice thickness was 1 mm for all views. The imaging parameters used were: repetition time (TR) of 3.25 s, time of echo (TE) of 60 ms.

Results and discussion

Synthesis and optical properties of CIS-rQDs

Indium-111 was absorbed and deposited on the interface layer of nonradioactive Cu-In-Se core following the formation of nonradioactive ZnS shell (Fig. 1a). The high radioactive reaction yield (>90%) and reproducibility of this synthetic strategy makes it a robust method to produce the intrinsically radioactive NPs not only limited to QDs. The multilayer ZnS shells prevent leakage of radionuclides from core of NPs and restore fluorescence after ligand exchange. Bio-stability of radionuclide in NPs was also greatly improved due to the high stability of ZnS in physiological condition,[35-37] which is beneficial to long-term *in vivo* trafficking of CIS-rQDs.

The fluorescent emission of Cu-In-Se/[111]InZnS QDs ranges from 650-850 nm with full width half-maximum of the peak (FWHM) about 120 nm (Fig. 1c), which is consistent with previous report.[32] The emission spectrum is in optical region for *in vivo* fluorescence imaging with less background interference. It is interesting to observe that the emission of core/shell CIS-rQDs slightly red-shift after doping indium-111. It is well known that the fluorescence of QDs is sensitive to the surface/interface defects.[38] In order to interpret the observed bath chromatic effect of CIS-rQDs, a series of shell-doping reaction of CuInSe/ZnS with various amount of indium was investigated. The emission red shifted from 710 nm to 740 nm as the doping amount of indium increased from 2.4 µg to 240 µg (Fig. S4). It is possible to further adjust the emission of CIS-rQDs to ideal spectra range for *in vivo* fluorescence imaging by doping with other elements, such as gallium.

The fluorescent QY of zwitterionic CIS-rQDs decreased slightly from ~24% to ~18% compared with hydrophobic CIS-rQDs after ligand exchange, which indicates formation of intact shell on the core. It was reported 1~2% fluorescence QY is acceptable for *in vivo* NIR fluorescence imaging due to the high sensitivity of fluorescence and deeper tissue penetration of NIR light.[39] Intensive *in vivo* and *ex vivo* fluorescence imaging (fluorescent signal from liver, spleen, tumor, skin, lymph nodes and other organs) of mice injected with CIS-rQDs (2.4 nmole) was acquired in this study, which verifies the application of NIR CIS-rQDs for fluorescence imaging.

Specific activity and fluorescent QY are two important parameters to determine the dose of CIS-rQDs for SPECT/fluorescence imaging and appropriate design/synthesis of rQDs needs to be considered. With improved specific activity/fluorescent QY, it is also feasible to reduce the dose of CIS-rQDs applied for SPECT/fluorescence imaging. Due to medium decay half-life of indium-111 (~2.8 days), 7 mCi (259 MBq) of [111]InCl$_3$ was used to synthesize indium-111 CIS-rQDs with specific activity of ~125 mCi (4625 MBq)/µmole for SPECT/fluorescence imaging. The whole radiation exposure was reduced because the radionuclide was introduced in the second step of core-shell synthesis and radioactive reaction yield/specific activity of rQDs was improved. From the fluorescence and autoradiography images of CIS-rQDs in solution before and after ligand exchange, no obvious fluorescent or radioactive signal loss was observed after surface

modification with multidentate zwitterionic ligands (Fig. 1e). This reflects the good protection of ZnS shell to radionuclide as well as CIS core.

The molar ratio of copper, indium and selenium composites in CIS-rQDs is related to the process of synthesis. At initial stage of reaction, CIS core is rich in indium (Cu/In≈ 1/2 for QDs emitting at 750 nm).[32] The molar ratio of Cu/In/Se in CIS core in this study was determined as 1/1.88/1.35 by ICP-OES, which is close to the result reported in literature. This could be also the reason of small size CIS-rQDs core (~ 2 nm, Fig. S1) was obtained during the synthesis, since growth reaction was terminated shortly after nucleation at initial stage of reaction. The low ratio of selenium in the whole composition reflects the existence of sulfur in CIS-rQDs. Based on measurement of TEM and ICP, the molar concentration of CIS-rQDs in solution can be also estimated, which is important for *in vitro* and *in vivo* studies.

Synthesis of multidentate zwitterionic ligands and ligand exchange

DHLA-sulfobetaine is an excellent bidentate zwitterionic ligand to make compact and highly hydrophilic NPs. The NPs functionalized with zwitterionic ligands reduced nonspecific interaction with serum proteins/cell membrane and improved bio-stability of NPs.[40,41] However, indium-based CIS-rQDs functionalized with bidentate zwitterionic ligands are stable in PBS for only one week under the ambient condition (Fig. 1d right). Therefore, we developed a strategy to synthesize multidentate zwitterionic ligands PAA-DHLA-sulfobetaine (Fig. 1b) and micro-emulsion system was used to perform ligand exchange.[42] Multidentate zwitterionic CIS-rQDs are highly stable in PBS (over six months) under the ambient condition (Fig. 1d left).

Fluorescent QY, stability, size, zeta potential of zwitterionic CIS-rQDs and nonspecific interaction with mouse plasma/cell membrane

The fluorescent QY of multidentate zwitterionic ligands coated CIS-rQDs was measured using NIR dye 1,1',3,3,3',3'-hexamethylindotricarbocyanine iodide as the standard. At 650 nm excitation wavelength, the QY of zwitterionic CIS-rQDs in water is considerable high (~18%), which is consistent with the QY of bidentate zwitterionic ligands coated CIS-rQDs. It is well known that hydrodynamic size (HD) and zeta potential of NPs potentially influence their *in vitro* and *in vivo* properties. It was reported that HD size of small QDs could increase from 4-7nm to 20-40 nm when amphiphilic polymer was used as the coating.[43] The compact Poly-thiol multidentate ligands coated QDs (5.5 nm) and imidazole-PEG multidentate ligands functionalized QDs (11.5 nm) were reported previously.[29,44] In our study, 15 nm of multidentate zwitterionic CIS-rQDs was obtained. Although the size of multidentate zwitterionic CIS-rQDs is slightly bigger than bidentate zwitterionic rQDs (~7.2 nm) (Fig. S2), HD size of multidentate zwitterionic CIS-rQDs still can be considered as compact. This is due to small size of inorganic core, tight chelation of ligands with surface of CIS-rQDs as well as the small molecular size of zwitterionic groups. The HD size of zwitterionic CIS-rQDs measured by DLS is also comparable to the result of GFC-HPLC. The retention time of multidentate zwitterionic CIS-rQDs (~15 nm) is similar to globular thyroglobulin protein (Mw: 667 KD, HD size: 18.8 nm).
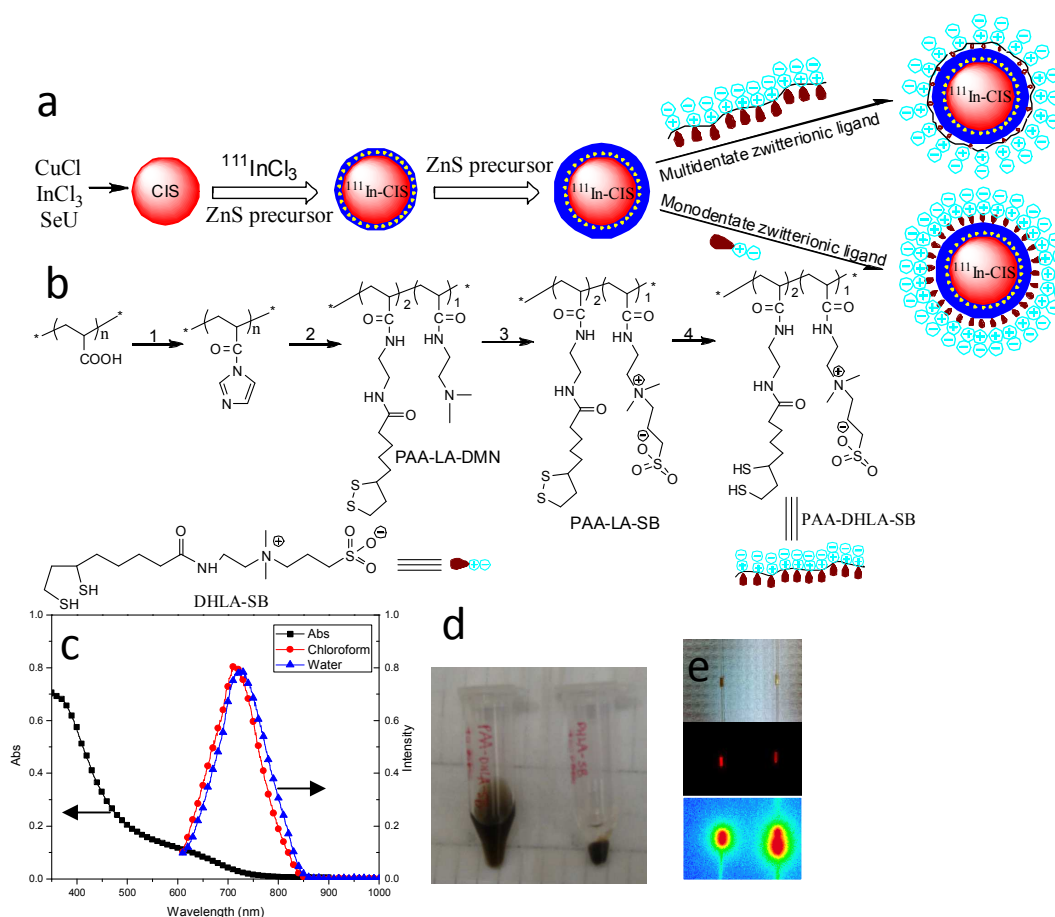
Fig. 1 (a) Synthetic scheme of multidentate or bidentate zwitterionic coated CIS-rQDs, which includes of CuInSe core synthesis, radiolabeling reaction followed shell synthesis and surface functionalization. (b) Synthetic scheme of multidentate zwitterionic polymer ligands PAA-DHLA-SB and chemical structure of bidentate zwitterionic ligands DHLA-SB. Reaction conditions: (1) CDI, THF, 4 °C to r.t., overnight; (2) N-(2-aminoethyl)-5-(1,2-dithiolan-3-yl)pentanamide, DMEDA, CHCl₃, r.t., overnight; (3) 1,3-propane sultone, CHCl₃, 60 °C, overnight; (4) NaBH₄, ethanol/H₂O, 4 °C to r.t. in 4 hrs. (c) UV-vis absorption (in chloroform) and fluorescence spectrum of CIS-rQDs (in chloroform and water). d) Photograph of multidentate zwitterionic CIS-rQDs (left) and bidentate zwitterionic CIS-rQDs (right) in PBS solution after one week storage at ambient condition. (e) Photograph of CIS-rQDs before (left) and after (right) functionalization with multidentate zwitterionic ligands: under bright light (top); under excitation of 650 nm (middle) and autoradiography (bottom).

It is surprising to observe a very negative zeta potential for both bidentate zwitterionic (DHLA-SB) CIS-rQDs (-79 mV) and multidentate zwitterionic (PAA-DHLA-SB) CIS-rQDs (-45 mV) in D.I water (Fig. S2). Theoretically the zwitterionic surface should show roughly neutral charge. We therefore studied the effect of PH/buffer to zeta potential of zwitterionic QDs. In PBS buffer (PH=7), the zwitterionic CIS-rQDs showed a slightly negative charge (zeta potential -6.86 mv at PH 7). The zeta potential changed from -0.15 mv to -14.7 mv when PH of PBS buffer increased from 2.1 to 11 (Fig. S3). This result shows significant influence of PH/ionic strength to the zeta potential of zwitterionic CIS-rQDs. Our result is also consistent to previous report by Han *et al.*[31] Although only one multidentate zwitterionic ligand (SB/DHLA=1/2) was used to functionalize CIS-rQDs in this study, previously we reported a strategy to tune surface charge density (zeta potential) of QDs with different multidentate zwitterionic polymer coating and the relation of cytotoxicity of zwitterionic QDs with their surface charge density.[42]

When NPs were applied for *in vitro*/*in vivo* imaging, it is crucial to reduce the nonspecific interaction of NPs with plasma proteins or cell membrane and minimize the opsonization effect. Binding of NPs with plasma proteins could result in clearance of NPs from circulation by immune system which decreases the possibility of delivering NPs to target tissues and enhances the accumulation in RES.[45] It has been reported that zwitterionic NPs are beneficial to reduce the nonspecific interaction with serum proteins and cell membrane.[41,42] The interaction of multidentate zwitterionic CIS-rQDs with mouse plasma was monitored by gel filtration chromatography (GFC). Multidentate zwitterionic CIS-rQDs were incubated with plasma at different time points (from 1 hr to 24 hrs). The robust radioactivity of CIS-rQDs can be detected by radio-detector of HPLC-GFC. The retention time (HD size) of multidentate zwitterionic CIS-rQDs did not change after 24 hrs incubation with plasma, indicating the reduced nonspecific interaction of zwitterionic CIS-rQDs with plasma proteins (Fig. S5). We also verified the reduced nonspecific binding of zwitterionic CIS-rQDs with cell membrane by fluorescent microscopy. No obvious fluorescence was observed from the COLO 205 or KB-3-1 cells after 24 hrs incubation of 15 nM or 75 nM CIS-QDs (Fig. S8), which reflects the low nonspecific binding of

zwitterionic CIS-rQDs with cell membrane. This result is also consistent to the cell uptake study by gamma counting, which showed low cellular uptake rate (0.2-0.4%, from 15 min to 24 hrs) and our previous study.[42]

Cell viability and cell uptake of COLO-205 and KB-3-1 treated with zwitterionic CIS-rQDs

The cell viability of COLO-205 and KB-3-1 cells was measured to demonstrate the cytotoxicity of zwitterionic CIS-rQDs. In our previous studies, it was found that COLO-205 and KB-3-1 cell lines showed different cytotoxic sensitivity to zwitterionic Cd-QDs.[42] The results showed that CIS-rQDs are non-toxic at the concentration of 100 nM for COLO-205 and 50nM for KB-3-1 cells up to 24 hr incubation (Fig. 2a). Compared with CIS-rQDs, zwitterionic cadmium-based QDs showed toxicity to KB-3-1 and COLO-205 cells at ~25 nM.[23,42] Reduced cytotoxicity of CIS-rQDs could be due to more stable chelation interaction of multidentate ligands with the surface of NPs as well as the elimination of highly toxic cadmium by indium-based CIS-rQDs. At this point, it is especially important to synthesize cadmium-free QDs for *in vivo* application. The cytotoxicity of CIS-rQDs is basically due to quantum dots/nanoparticles since no cytotoxicity was observed for zwitterionic polymer up to 10 μM (Fig. S6).

The cell uptake of CIS-rQDs in COLO-205 and KB-3-1 with time was quantitatively investigated by gamma counting (Fig. 2b). A low uptake rate of zwitterionic CIS-rQDs was found for both of two carcinoma cell lines (0.2% at 15 min and 0.4% at 24 hrs, Fig. S7). Numbers of CIS-rQDs taken up by COLO-205 or KB-3-1 cells is about 1×10^5 CIS-rQDs/cell at 15 min. Prolonged incubation of cells with CIS-rQDs up to 24 hrs resulted in gradual increase of uptake (~2×10^5 CIS-rQDs/cell) compared with the data at 15 min. Since zwitterionic CIS-rQDs are untargeted NPs, passive uptake process could be the most possible mechanism. It had been reported that compact cysteamine coated zwitterionic QDs or glutathione/cysteamine coated zwitterionic gold NPs could penetrate (absorb) through (on) cell membrane without destroying cell membrane and inducing cytotoxicity.[46,47] The zwitterionic surface and compact size could be the most important factors determining the passive uptake of CIS-rQDs by cells. Low cell uptake rate of zwitterionic CIS-rQDs probably due to reduced nonspecific interaction of zwitterionic surface of CIS-rQDs with negative cell membrane compared with other small inorganic NPs as nanoceria or gold NPs.[48-50]

In vivo SPECT/fluorescence imaging and accumulation of CIS-rQDs in tumor

One COLO-205 tumor bearing nude mouse with high tumor uptake in the group was selected to demonstrate *in vivo* SPECT/fluorescence imaging of zwitterionic CIS-rQDs (Fig. 3). SPECT imaging provided semi-quantitative information of *in vivo* distribution of zwitterionic CIS-rQDs with the time (6 hrs, 24 hrs and 48 hrs) by region of interest (ROI) analysis. At 48 hrs post injection of zwitterionicrQDs, besides liver (18.4%ID/g), spleen (8.4%ID/g) and lungs (2.6%ID/g), tumor showed high uptake of zwitterionic CIS-rQDs (4.6%ID/g, from ROI analysis). The accumulation of untargeted CIS-rQDs in tumor is due to the enhanced permeability and retention (EPR) effect due to leaky neovasculature. The compact size of zwitterionic CIS-rQDs (~15 nm) and low nonspecific interaction with plasma could make the NPs rapidly penetrate/diffuse through the leaky neovasculature of tumor tissue at 6 hrs (reach to ~3.0%ID/g) and improved accumulation of CIS-rQDs in tumor was observed with time (~4.0%ID/g at 24 hrs) due to lack of effective lymphatic drainage of tumor. The clearance of zwitterionic CIS-rQDs from heart and lungs (%ID/g dropped from 5.3 to 1.4 from heart, and 5.4 to 2.6 from lungs) with time was also observed from SPECT imaging/ROI analysis. *In vivo* stability of intrinsically radiolabeled CIS-rQDs was further confirmed by SPECT/fluorescence imaging. After 48 hrs, the SPECT and fluorescence imaging correlate with each other. This reflects the colocalization of radioactive signal with fluorescent signal of CIS-rQDs and verified excellent *in vivo* stability of intrinsic radiolabeled CIS-rQDs. Improved bio-stability of CIS-rQDs makes it a good probe for long-term trafficking and imaging. Detailed data from ROI analysis of *in vivo* SPECT results are listed in Table S1. The analysis of ex vivo fluorescence image showed higher liver (47.4%) and tumor uptake (11.5%) (Fig. S9). However, the fluorescence imaging usually was not considered as a quantitative imaging modality.

Significant different uptake/accumulation of zwitterionic CIS-rQDs in tumors from different mice was observed. It is well known that the passive uptake of NPs depends on the size/surface of NP as well as development of neovasculature structure of tumor. The relation between accumulation of CIS-rQDs and leaky vasculature of tumor was studied by *in vivo*
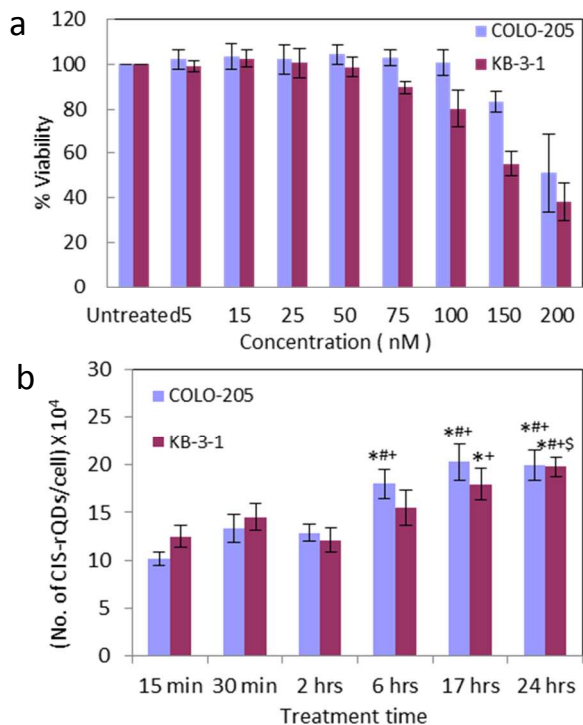
Fig. 2 (a) Cell viability of COLO-205 and KB-3-1 cells incubated with CIS-rQDs for 24 hrs, evaluated using Cell Titer-Glo cell viability assay kit. Data is expressed as % Viability in treated groups compared to untreated (100% viability) ± S.D. *P<0.05 compared to control. (b) Cell uptake data showing No. of CIS-rQDs/cell of 15 nM multidentate zwitterionic CIS-rQDs at various time points in COLO-205 and KB-3-1 cell lines. Data is expressed as No. of CIS-rQDs/cell ± Std Error. Fisher's PLSD test was done to evaluate statistical difference in uptake between each time points. *,#,+ and $ indicate statistical differnce in uptake at indicated time points compared with 15 min, 30 min, 2 hrs and 6 hrs respectively.
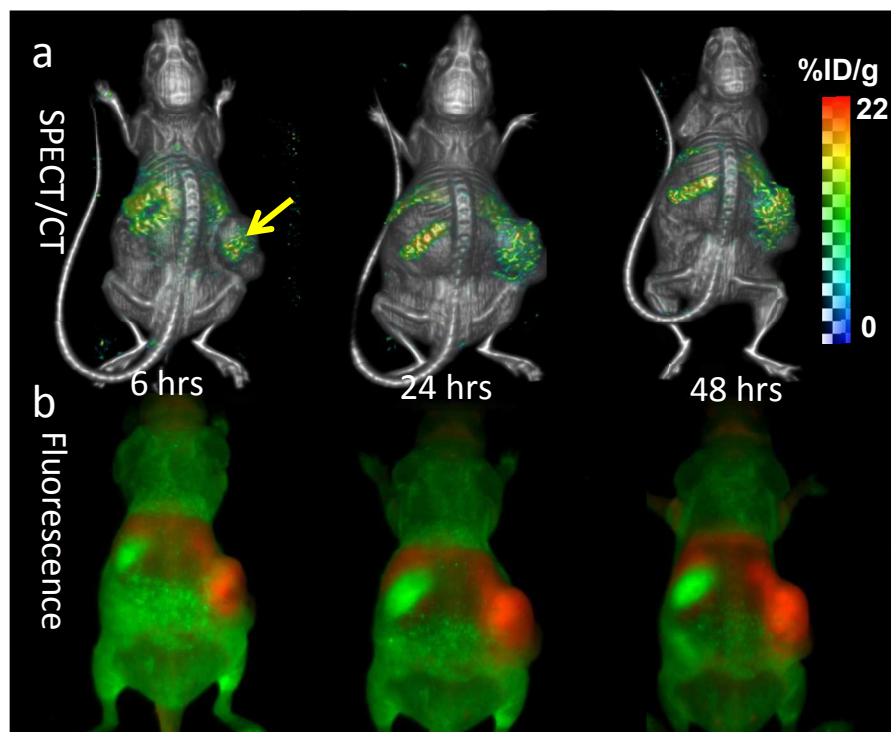
Fig.3 *In vivo* (a) SPECT/CT and (b) fluorescence imaging of the nude mouse bearing COLO-205 tumor post-injection (2.4 nmole zwitterionic CIS-rQDs, 300 μCi) at 6 hrs, 24 hrs and 48 hrs showed gradual passive accumulation of CIS-rQDs in the tumor reaching a maximum of 4.6% ID/g (from ROI analysis) at 48 hrs (The arrow points the tumor site). Similar trend could also be seen with the fluorescent signal from the tumor in this mouse.

MRI and *ex vivo* fluorescence image of tumor (Fig. 4). T2 weighted MRI image of tumor was acquired to verify the interstitial fluid level in the tumors, which reflects the development of leaky neovasculature and poor lymphatic drainage. It is obvious that CIS-rQDs showed highest uptake (4.6 %ID/g from ROI analysis of SPECT) in one COLO-205 tumor (left) which developed highly leaky vasculature with high interstitial fluid level. Lower fluid leveled tumor structure (right) showed resistance to the diffusion of nanoparticles and accompanied with decreased uptake rate of CIS-rQDs (0.3 %ID/g). The neovasculature of tumors is an important factor to determine the penetration/diffusion and accumulation of NPs. For example, previous reports have indicated that smaller pore size in certain tumor vasculatures could even inhibit the extravasation of compact QDs (20-25 nm).[51] The diffusion, retention, localization of CIS-rQDs influenced by microenvironment of tumor needs to be further studied to understand how to design the nanoprobes for imaging/therapy applications.

Combining fluorescence and gamma ray emitting moiety into a single nanoprobe provides the feasibility for quantitative investigation of biodistribution and pharmacokinetics *in vivo*. The intrinsically radiolabeled strategy demonstrated here, also provides the platform for further surface modification without interfering the design and synthesis of radioactive NPs for multimodal molecular imaging. Incorporation of radiation therapeutic isotopes (such as Cu-67) into rQDs, will extend the applications of these rQDs for radiation therapy. Three-dimensional images acquired from SPECT/CT reflected the whole-body biodistribution of zwitterionic CIS-rQDs with time. Optimal surface modification of CIS-rQDs with multidentate
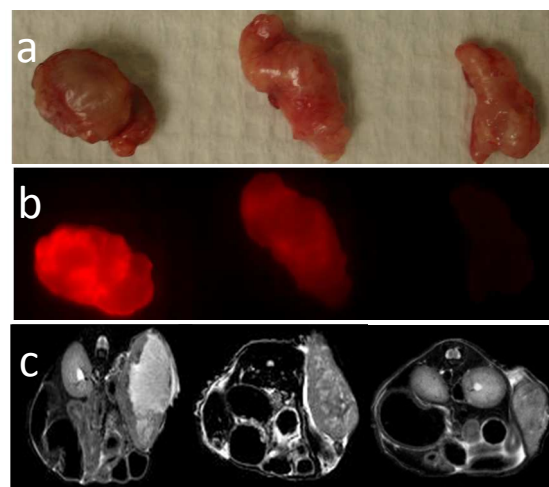

Fig.4 The accumulation of CIS-rQDs was related to the level of fluid inside the tumors, which indicates leaky vasculature and poor drainage. (a) Photograph of excised tumors, (b) *ex vivo* fluorescence imaging of tumors from different mice and (c) *in vivo* T2 weighted MR images of tumors. The fluorescent signal was highest in the first tumor (from the mouse in Fig. 3, the leftmost in this picture, which also had high levels of fluid accumulation in the tumor, moderate fluid accumulation in the second tumor (middle), while the third tumor on the right did not have fluid and the CIS-rQDs accumulation was also low, supporting the idea that the CIS-rQDs passively accumulated in the first and second tumors due to leaky vasculature.

zwitterionic coating is a strategy for improving stability and reducing plasma binding of CIS-rQDs *in vivo*. Complementary of SPECT/fluorescence modalities provides highly sensitive, deep tissue penetrated and quantitative imaging.

Conclusions

In this paper, we demonstrated the synthesis and surface functionalization of intrinsically In-111 radiolabeled NIR CIS-rQDs for bimodal SPECT/fluorescence imaging. To our best knowledge, this is the first paper to report about synthesis of highly stable, intrinsically radioactive CIS-rQDs for *in vivo* SPECT/fluorescence imaging. Multidentate zwitterionic polymer ligands were designed and synthesized to functionalize CIS-rQDs to improve the *in vivo* stability and reduce the interaction of CIS-rQDs with plasma proteins. Due to the unique surface functionalization, compact HD size and low toxic composition, cytotoxicity of multidentate zwitterionic CIS-rQDs was reduced. Passive accumulation of zwitterionic CIS-rQDs in tumor was verified from *in vivo* SPECT/fluorescence imaging due to EPR effect. Maximum of 4.6%ID/g uptake of zwitterionic CIS-rQDs in a COLO-205 tumor with highly developed leaky neovasculature was observed. The combination of SPECT with fluorescence modality makes the zwitterionic CIS-rQDs a promising nanoprobe for bimodal *in vivo* detection.

Acknowledgements

Notes and references

Center for Molecular Imaging, Department of Radiology, Virginia Commonwealth University, Richmond, VA 23298, United States.

†Electronic Supplementary Information (ESI) available: [TEM images of In-QDs, DLS/Zeta potential of bidentate and multidentate zwitterionic ligands coated In-rQDs, PH effect on zeta potential of zwitterionic CIS-QDs, fluorescent spectra of indium doped QDs, stability study of In-rQDs incubated with mouse plasma, cell uptake percentage by gamma counting, cell viability study of multidentate zwitterionic polymer, fluorescence microscopy of COLO 205 and KB-31 cell lines with zwitterionic CIS-rQDs, *ex vivo* fluorescence imaging of mouse organs and ROI analysis data of SPECT imaging.]. See DOI: 10.1039/b000000x/

1 D. W. Townsend.*J. Nucl. Med.*, 2008, **49**, 938 and references there.

2 J. Xie, K. Chen, J. Huang, S. Lee, J. Wang, J. Gao, X. Li and X. Chen. *Biomaterials*, 2010, **31**, 3016.

3 S. T. Selvan, P. K. Patra, C. Y. Ang and J. Y. Ying, *Angew.Chem.*, 2007, **119**, 2500.

4 N. Insin, J. B. Tracy, H. Lee, J. P. Zimmer, R. M. Westervelt and M. G. Bawendi, *ACS Nano*, 2008, **2**, 197.

5 C. Glaus, R. Rossin, M. J. Welch and G. Bao, *Bioconjugate.Chem.*, 2010, **21**, 715.

6 C. Alric, J. Taleb, G. L. Duc, C. Mandon, C. Billotey, A. L. Meur-Herland, T. Brochard, F. Vocanson, M. Janier, P, Perriat, S. Roux and O. Tillement. *J. Am. Chem. Soc.*, 2008, **130**, 5908.

7 M. F. Kircher, A. Zerda, J. V. Jokerst, C. L. Zavaleta, P. J. Kempen, E. Mittra, K. Pitter, R. Huang, C. Campos, F. Habte, R. Sinclair, C. W. Brennan, I. K. Mellinghoff, E. C. Holland and S. S. Gambhir. *Nat. Med.*, 2012, **18**, 829.

8 M. Bruchez, M. Moronne, P. Gin, S. Weiss and A. P. Alivisatos, *Science*, 1998, **281**, 2013.

9 W. C. W. Chan and S. M. Nie, *Science*, 1998, **281**, 2016.

10 X. Michalet, F. F. Pinaud, L. A. Bentolila, J. M. Tsay, S. Doose, J. J. Li, G. Sundaresan, A. M. Wu, S. S. Gambhir and S. Weiss. *Science*, 2005, **307**, 538.

11 W. J. M. Mulder, R. Koole, R. J. Brandwijk, G. Storm, P. T. K. Chin, G. J. Strijkers, C. M. Donegá, K. Nicolay and A. W. Griffioen. *NanoLett.*, 2006, **6**, 1.

12 T. Jin, Y. Yoshioka, F. Fujii, Y. Komai, J. Seki and A. Seiyama, *Chem. Commun.*, 2008, **44**, 5764.

13 G. J. Stasiuk, S. Tamang, D. Imbert, C. Poillot, M. Giardiello, C. Tisseyre, E. L. Barbier, P. H. Fries, M. Waard, P. Reiss and M. Mazzanti. *ACS Nano*, 2011, **5**, 8193.

14 W. B. Cai, K. Chen, Z. B. Li, S. S. Gambhir and X. Y. Chen. *J. Nucl. Med.*, 2007, **48**, 1862.

15 F. Ducongé, T. Pons, C. Pestourie, L. Hérin, B. Thézé, K. Gombert, B. Mahler, F. Hinnen, B. Kühnast, F. Dollé, B. Dubertret, and B. Tavitian. *Bioconjugate Chem.*, 2008, **19**, 1921.

16 L. Li, T. J. Daou, I. Texier, T. T. K. Chi, N. Q. Liem, P. Reiss, *Chem. Mater.*, 2009, **21**, 2422.

17 J. H. Gao, K. Chen, R. G. Xie, J. Xie, Y. J. Yan, Z. Cheng, X. G. Peng and X. Y. Chen. *Bioconjugate Chem.*, 2010, **21**, 604.

18 P. M. Allen, W. H. Liu, V. P. Chauhan, J. M. Lee, A. Y. Ting, D. Fukumura, R. K. Jain and M. G. Bawendi. *J. Am. Chem. Soc.*, 2010, **132**, 470.

19 K-T.Yong, I. Roy, H. Ding, E. J. Bergey and P. N. Prasad.*Small*, 2009, **5**, 1997.

20 Y-P.Gu, R. Cui, Z-L. Zhang, Z-X.Xie and D-W.Pang, *J. Am. Chem. Soc.*, 2012, **134**, 792.

21 Y. Zhang, G. Hong, Y. Zhang, G. Chen, F. Li, H. Dai and Q. Wang.*ACS Nano*, 2012, **6**, 3695.

22 C. Tu, X. Ma, A. House, S. M. Kauzlarich and A. Y. Louie. ACS *Med. Chem. Lett.*, 2011, **2**, 285.

23 M. H. Sun, D. Hoffman, G. Sundaresan, L. Yang, N. Lamichhane and J. Zweit, *Am. J. Nucl. Med. Mol. Imaging*, 2012, **2**, 122.

24 L. K. Yang, G. Sundaresan, M. H. Sun, P. Jose, D. Hoffman, P. R. McDonaph, N. Lamichhane, C. S. Cutler, J. M. Perez and J. Zweit. *J. Mater. Chem. B*, 2013, **1**, 1421.

25 Z-J.Zhu, Y-C.Yeh, R. Tang, B. Yan, J. Tamayo, R. W. Vachet and V. M. Rotello.Nat. chem., *2011*, **3**, 963.

26 Y. Wu, S. Chakrabortty, R. A. Gropeanu, J. Wilhelmi, Y. Xu, K. S. Er, S. L. Kuan, K. Koynov, Y. Chan and T. Weil. *J. Am. Chem. Soc.*, 2010, **132**, 5012.

27 Z. Krpetić, P. Nativo, F. Porta and M. Brust, *Bioconjugate Chem.*, 2009, **20**, 619.

28 H. B. Na, G. Palui, J. T. Rosenberg, X. Ji, S. C. Grant and H. Mattoussi, *ACS Nano*, 2012, **6**, 389.

29 W. Liu, A. B. Greytak, J. Lee, C. R. Wong, J. Park, L. F. Marshall, W. Jiang, P. N. Curtin, A. Y. Ting, D. G. Nocera, D. Fukumura, R. K. Jain and M. G. Bawendi. *J. Am. Chem. Soc.*, 2010, **132**, 472.

30 S. Impellizzeri, B. McCaughan, J. F. Callan and F. M. Raymo, *J. Am. Chem. Soc.*, 2012, **134**, 2276.

31 H-S. Han, J. D. Martin, J. Lee, D. K. Harris, D. Fukumura, R. K. Jain and M. Bawendi. *Angew. Chem. Int. Ed.*, 2013, **52**, 1414.

32 E. Cassette, T. Pons, C. Bouet, M. Helle, L. Bezdetnaya, F. Marchal and B. Dubertret. *Chem. Mater.*, 2010, **22**, 6117.

33 T. Pons, E. Pic, N. Lequeux, E. Cassette, L. Bezdetnaya, F. M. Guillemin and B. Dubertret. *ACS Nano*, 2010, **4**, 2531.

34 L. Li, T. J. Daou, I. Texier, T. T. K. Chi, N. Q. Liem and P. Reiss, *Chem. Mater.*, 2009, **21**, 2422.

35 A. M. Derfus, W. C. W. Chan and S. N. Bhatia, *NanoLett.*, 2004, **4**, 11.

36 C. Kirchner, T. Liedl, S. Kudera, T. Pellegrino, A. M. Javier, H. E. Gaub, S. Stöelzle, N. Fertig and W. J. Parak. *NanoLett.*, 2005, **5**, 331.

37 R. A. Hardman, *Environ. Health.Persp.*, 2006, **114**, 165.

38 W. K. Bae, K. Char, H. Hur and S. Lee, *Chem. Mater.*, 2008, 20, 531.

39 J. P. Zimmer, S-W. Kim, S. Ohnishi, E. Tanaka, J. V. Frangioni and M. G. Bawendi, *J. Am. Chem. Soc.*, 2006, **128**, 2526.

40 H. S. Choi, W. Liu, P. Misral, E. Tanakal, J. P. Zimmer, B. I. Ipe, M. G. Bawendi and J. V. Frangioni. *Nat. Biotechnol.*, 2007, **25**, 1165.

41 E. Muro, T. Pons, N. Lequeux, A. Fragola, N. Sanson, Z. Lenkei and B. Dubertret. *J. Am. Chem. Soc.*, 2010, **132**, 4556.

42 M. H. Sun, L. K. Yang, P. Jose, L. Wang and J. Zweit, *J. Mater. Chem. B*, 2013, **1**, 6137.

43 W. W. Yu, E. Chang, J. C. Falkner, J. Zhang, A. M. Al-Somali, C. M. Sayes, J. Johns, R. Drezek, V. L, Colvin. *J. Am. Chem. Soc.*, 2007, **129**, 2871.

44 A. M. Smith and S. Nie, *J. Am. Chem. Soc.*, 2008, **130**, 11278.

45 M. L. Schipper, G. Iyer, A. L. Koh, Z. Cheng, Y. Ebenstein, A. Aharoni, S. Keren, L. A. Bentolila, J. Li, J. Rao, X. Chen, U. Banin, A. M. Wu, R. Sinclair, S. Weiss and S. S. Bambhir. *Small*, 2009, **5**, 126.

46 T. Wang, J. Bai, X. Jiang and G. U. Nienhaus, *ACS Nano*, 2012, **6**, 1251.

47 M. Yu, C. Zhou, J. Liu, J. D. Hankins and J. Zheng, *J. Am. Chem. Soc.*, 2011, **133**, 11014.

48 F. Simonelli, P. Marmorato, K. Abbas, J. Ponti, J. Kozempel, U. Holzwarth, F. Franchini and F. Rossi. *IEEE Trans. Nanobiosci.*, 2011, **10**, 44.

49 J. I. Cutler, K. Zhang, D. Zheng, E. Auyeung, A. E. Prigodich and C. A. Mirkin, *J. Am. Chem. Soc.*, 2011, **133**, 9254.

50 X. Li, H. Zhou, L. Yang, G. Du, A. S. Pai-Panandiker, X. Huang and B. Yan. *Biomaterials*, 2011, **32**, 2540.

51 B. R. Smith, Z. Cheng, A. De, J. Rosenberg and S. S. Gambhir, *Small*, 2010, **6**, 2222.

A highly stable bimodal indium(111) radiolabeled indium QDs were synthesized for in vivo SPECT/fluorescence imaging.